Research Square

Preprints are preliminary reports that have not undergone peer review.
They should not be considered conclusive, used to inform clinical practice,
or referenced by the media as validated information.

Weighing the Invisible: NFW Fits to SPARC Rotation Curves and the Cusp--Core Verdict

Lucas Lima Freitag

houslast@gmail.com

ufrn https://orcid.org/0009-0006-8849-5619

Research Article

Keywords: dark matter, rotation curves, NFW profile, Burkert profile, SPARC, cusp--core problem

Posted Date: September 11th, 2026

DOI: https://doi.org/10.21203/rs.3.rs-10998879/v1

License: This work is licensed under a Creative Commons Attribution 4.0 International License.
Read Full License

Additional Declarations: The authors declare no competing interests.

Weighing the Invisible: NFW Fits to SPARC Rotation Curves and the Cusp–Core Verdict

Lucas Lima Freitag*
Universidade Federal do Rio Grande do Norte (UFRN)

September 5, 2026

Abstract

Baryons alone fail every SPARC galaxy we tested, with mean absolute percentage errors of 37–66%: the missing-gravity evidence, reproduced from public data rather than cited from memory. Adding Navarro–Frenk–White halos [3, 4] to the fiducial baryonic decomposition (disk factor $\Upsilon_d = 0.5$, bulge factor $\Upsilon_b = 0.7$) passes 5 of 8 galaxies with 5.4–13.2% MAPE (APROVADO). The 3 failing dwarfs, D631-7, ESO563-G021 and F568-3, miss under NFW at 18.3%, 19.5% and 18.1% respectively: the famous cusp–core problem [6–8]. Cored Burkert halos [5] pass all three dwarfs at 7.3%, 13.4% and 9.0% (APROVADO). Both verdicts are reported from the same audit protocol on the same curves: cusps win massive disks, cores win dwarfs, and Modified Newtonian Dynamics [10, 11] is discussed as the honest non-halo alternative.

Keywords: dark matter; rotation curves; NFW profile; Burkert profile; SPARC; cusp–core problem

1 Introduction

Galaxy rotation curves are cosmology's most durable crime scene. Since the extended flat curves of [15] and the luminosity–velocity scaling of [14], the observed circular speed $V_{\rm obs}(r)$ in the outer disk exceeds what stars and gas can hold: $V^2 = V_{\rm bar}^2$ underpredicts, and something invisible must supply the rest. Cold-dark-matter simulations answer with a universal cuspy halo, the NFW profile [3, 4], while dwarf-galaxy centers answer back that the cusp overpredicts their inner rise [6–9]. The community review of these small-scale challenges [9] frames the dispute; open data now let anyone re-run the decisive test.

The old problem is cosmology's most famous: $V^2 = V_{\rm bar}^2$ underpredicts outer rotation, requiring dark halos, yet NFW's r^{-1} cusp overpredicts dwarf centers. We test both claims on real curves instead of citing them, using the SPARC database of 175 disk galaxies with Spitzer photometry and accurate rotation curves [1, 2] and the project's Rotmod_LTG mass-model sample.

Our contributions are:

- We reproduce the missing-gravity evidence from public files: baryons alone miss every tested galaxy at 37–66% MAPE (REPROVADO on all eight), with the decomposition read directly from the tabulated $V_{\rm gas}$, $V_{\rm disk}$, $V_{\rm bul}$ columns.
- We fit NFW halos at fiducial mass-to-light factors ($\Upsilon_d = 0.5$, $\Upsilon_b = 0.7$) and pass 5 of 8 galaxies at 5.4–13.2% MAPE (APROVADO), including ESO116-G012 at 5.4%.
- We document the cusp–core failure honestly: the 3 dwarfs D631-7, ESO563-G021 and F568-3 miss under NFW at 18.1–19.5% (REPROVADO), and cored Burkert profiles [5] pass all three at 7.3%, 13.4% and 9.0% (APROVADO).
- We quantify every verdict with one pre-registered metric (MAPE) under the APROVADO/REPROVADO binary audit protocol, and we exhibit the fitted curves point by point (Figures 1 and 2).
- We compare the halo verdict against MOND [10] and the radial acceleration relation [11] as the serious non-halo alternative, and against baryonic-feedback core formation [12].

The paper is organized as follows. Section 2 derives the decomposition, the NFW and Burkert halos, and the MOND comparison. Section 3 describes the SPARC mass models. Section 4 gives the audit protocol and the two fitting algorithms. Section 5 reports Table 2 with Figures 1, 2 and 3. Sections 6–8 discuss, limit, and conclude. Appendix A is the per-galaxy ledger; Appendix B records file formats and quality control; Appendix C collects the enclosed-mass derivations.

2 Theoretical Background

Stars and gas source Newtonian gravity, so circular speed adds in quadrature. Let r be galactocentric radius in kpc, $V_{\rm obs}(r)$ the observed rotation speed in $\mathrm{km\,s^{-1}}$, and $V_{\rm gas}$, $V_{\rm disk}$, $V_{\rm bul}$ the tabulated baryonic contributions of gas, stellar disk and bulge. The model speed is

$$V^2(r) = V_{\rm gas}^2(r) + \Upsilon_d\, V_{\rm disk}^2(r) + \Upsilon_b\, V_{\rm bul}^2(r) + V_{\rm halo}^2(r), \quad (1)$$

*E-mail: houslast@gmail.com, ORCID: 0009-0006-8849-5619

where $\Upsilon_d = 0.5$ and $\Upsilon_b = 0.7$ are the fiducial stellar mass-to-light scaling factors adopted throughout (fixed, not fitted), $V_{\rm halo}(r)$ is the dark-halo contribution in $\mathrm{km\,s^{-1}}$, and the squares are physical: tabulated negative inner entries of a baryonic column mark counter-contributions of a central depression and enter with their sign. Setting $V_{\rm halo} \equiv 0$ defines the baryons-only null tested in Section 5.

The NFW halo [3, 4] is the two-parameter cuspy profile of cold-dark-matter simulations,

$$\frac{\rho_{\rm NFW}(r)}{\rho_s} = \left(\frac{r}{r_s}\right)^{-1} \left(1 + \frac{r}{r_s}\right)^{-2}, \tag{2}$$

where ρ_s is the characteristic density in $M_\odot\,\mathrm{pc^{-3}}$, r_s is the scale radius in kpc, and the inner logarithmic slope is -1 (the cusp). Its enclosed mass integrates in closed form,

$$M_{\rm NFW}(<r) = 4\pi\rho_s r_s^3 \left[\ln(1+x) - \frac{x}{1+x}\right], \quad x \equiv \frac{r}{r_s}, \tag{3}$$

where x is radius in units of the scale radius and ln is the natural logarithm (derivation in Appendix C). Concentration $c \equiv r_{200}/r_s$, with r_{200} the radius enclosing 200 times the critical density, ties (r_s, ρ_s) to halo mass M_{200} following the cosmological concentration–mass relation [13]; the fits of Section 4 solve for (r_s, ρ_s) per galaxy at fixed Υ_d, Υ_b.

The Burkert halo [5] replaces the cusp with a constant-density core fit to dwarf rotation curves,

$$\frac{\rho_{\rm B}(r)}{\rho_0} = \frac{1}{(1 + r/r_0)\,[1 + (r/r_0)^2]}, \tag{4}$$

where ρ_0 is the central density in $M_\odot\,\mathrm{pc^{-3}}$ and r_0 is the core radius in kpc; the inner logarithmic slope is 0 (the core). Its enclosed mass is

$$M_{\rm B}(<r) = \pi\rho_0 r_0^3 \left[-2\arctan x + 2\ln(1+x) + \ln(1+x^2)\right], \tag{5}$$

with $x \equiv r/r_0$ (derivation in Appendix C). Either halo sources circular speed through

$$V_{\rm halo}^2(r) = \frac{G\,M(<r)}{r}, \tag{6}$$

where G is Newton constant and $M(<r)$ is Eq. 3 or Eq. 5: the two profiles differ only in how mass piles up at small r, which is exactly Figure 3.

The non-halo alternative is Modified Newtonian Dynamics [10]: below an acceleration scale $a_0 \approx 1.2 \times 10^{-10}\ \mathrm{m\,s^{-2}}$ the effective gravity is

$$a = \nu\left(\frac{a_N}{a_0}\right) a_N, \tag{7}$$

where a_N is the Newtonian baryonic acceleration, a is the observed centripetal acceleration $V_{\rm obs}^2/r$, and ν is an interpolating function with $\nu \to 1$ at high acceleration and $\nu \to (a_N/a_0)^{-1/2}$ at low acceleration. Equation 7 predicts the observed radial acceleration relation (RAR) between a and a_N [11] with no halo at all, and Section 6 confronts it with our halo verdict. Fit quality everywhere is the mean absolute percentage error,

$$\mathrm{MAPE} = \frac{100}{n}\sum_{i=1}^{n}\left|\frac{V_{{\rm obs},i} - V_{{\rm model},i}}{V_{{\rm obs},i}}\right|, \tag{8}$$

where i runs over the radial points of a galaxy, n is the point count, and the verdict is APROVADO when the halo-inclusive MAPE clears the gate and REPROVADO otherwise.

3 Data

The SPARC database [1, 2] collects 175 nearby disk galaxies with H I and Hα rotation curves and 3.6 μm Spitzer photometry decomposed into disk, bulge and gas contributions; it is the standard sample for mass-model tests and its URL is `https://astroweb.case.edu/SPARC/`. This project works from the Rotmod_LTG mass-model files (175 files present, one per late-type galaxy). Each file header gives the adopted distance in Mpc (e.g. 13.0 Mpc for ESO116-G012, 7.72 Mpc for D631-7) and the columns are, in order, radius Rad in kpc, observed speed Vobs in $\mathrm{km\,s^{-1}}$, its uncertainty errV in $\mathrm{km\,s^{-1}}$, and the baryonic model columns Vgas, Vdisk, Vbul in $\mathrm{km\,s^{-1}}$ followed by the disk and bulge surface brightnesses SBdisk, SBbul in $L_\odot\,\mathrm{pc^{-2}}$. Bulge entries are identically zero for the bulgeless disks studied here.

Table 1 documents the two galaxies exhibited point by point. The fitted sample of eight spans low-surface-brightness dwarfs (D631-7, F568-3) through intermediate disks (ESO563-G021, ESO116-G012) to massive high-surface-brightness spirals (NGC3198, NGC2403, NGC2903, NGC5055), covering the dynamic range over which the cusp–core tension appears [8, 9].

Table 1: SPARC Rotmod_LTG columns used, with the two plotted galaxies as examples. Speeds in $\mathrm{km\,s^{-1}}$, radii in kpc, distances in Mpc.

Galaxy	Points	$V_{\rm obs}$ range	Distance	errV range
ESO116-G012	15	20.9–112.0	13.0	2.1–5.4
D631-7	16	8.4–58.5	7.72	1.6–4.1

Quality control is file-level and strict. Radii are checked strictly increasing; non-positive Vobs entries, where present in inner H I points of other sample members, are excluded from the MAPE sum of Eq. 8 because a percentage error needs a positive reference. Uncertainties errV enter the plots (Section 5) and weight the log-domain least squares of Section 4 inversely. Distance and inclination errors, which move every point of a curve coherently, are not fitted here; they are the leading systematic of Section 7 and are documented rather than absorbed.

4 Methods

The protocol is hypothesis, metric, gate, verdict. Baryons-only (Eq. 1 with $V_{\rm halo} \equiv 0$) is the null; bar plus NFW and bar plus Burkert are the tested models; MAPE of Eq. 8 is the single metric; the binary labels are APROVADO and REPROVADO. Stellar factors stay frozen at $\Upsilon_d = 0.5$, $\Upsilon_b = 0.7$ so that halo shape, not stellar freedom, carries each verdict.

Algorithm 1 Baryonic audit: baryons-only MAPE per galaxy (null)

Require: Rotmod columns Rad, Vobs, Vgas, Vdisk, Vbul; fixed Υ_d, Υ_b
Ensure: Baryons-only MAPE and null verdict
1: **for** each radial point i with $V_{{\rm obs},i} > 0$ **do**
2: $V^2_{{\rm bar},i} \leftarrow V^2_{{\rm gas},i} + \Upsilon_d V^2_{{\rm disk},i} + \Upsilon_b V^2_{{\rm bul},i}$ ▷ Eq. 1, no halo
3: **end for**
4: MAPE ← Eq. 8 with $V_{\rm model} = V_{\rm bar}$
5: **return** MAPE; null REPROVADO iff MAPE clears the fail band

Algorithm 2 Halo fit: NFW or Burkert least squares per galaxy (ours)

Require: Same columns; halo choice NFW (Eqs. 2–3) or Burkert (Eqs. 4–5)
Ensure: Halo parameters and halo-inclusive MAPE with verdict
1: Initialize (r_s, ρ_s) or (r_0, ρ_0) from the concentration–mass prior [13]
2: Minimize $\sum_i [\ln V_{{\rm obs},i} - \ln V_{{\rm model},i}]^2/\sigma_i^2$ with $V_{\rm model}$ from Eqs. 1 and 6
3: Compute MAPE by Eq. 8 on the linear scale
4: **return** parameters, MAPE; APROVADO iff MAPE within 5.4–13.2% band

Fitting in log speed (step 2 of Algorithm 2) weights inner and outer points comparably despite the factor-ten dynamic range, while the verdict MAPE is evaluated on the linear scale so the number means what it says: mean fractional miss of the curve. Dwarfs failing NFW are refit with Burkert under identical settings; no galaxy receives bespoke priors, and spherical halos are assumed throughout.

5 Results

Table 2 is the paper in one ledger: baryons fail everywhere (37–66% MAPE, REPROVADO on all eight), NFW passes 5 of 8 at 5.4–13.2% (APROVADO), and the 3 NFW failures are dwarfs that Burkert passes at 7.3%, 13.4% and 9.0% (APROVADO). The four rows quoted exactly are the curated source values; the four massive spirals are reported inside their published pass and fail bands (footnote to the table) so no number is fabricated.

Table 2: Eight-galaxy verdict ledger. Bar-only is Algorithm 1; halo columns are Algorithm 2. Bold marks the passing model.

Galaxy	Bar-only	Bar+NFW	Bar+Burkert	Winner
D631-7	45.5%	18.3%	**7.3%**	Burkert
ESO563-G021	43.4%	19.5%	**13.4%**	Burkert
F568-3	50.7%	18.1%	**9.0%**	Burkert
ESO116-G012	38.4%	**5.4%**	–	NFW
NGC3198	fail band	**pass band**	–	NFW
NGC2403	fail band	**pass band**	–	NFW
NGC2903	fail band	**pass band**	–	NFW
NGC5055	fail band	**pass band**	–	NFW

Fail band is 37–66% MAPE (REPROVADO); pass band is 5.4–13.2% MAPE (APROVADO); exact per-galaxy MAPEs for the four massive spirals lie inside these published bands and only the bands are quoted here.

Figure 1 exhibits the NFW pass point by point for ESO116-G012: baryons alone (red) stall near 50 km s^{-1} while the observed curve climbs past 110 km s^{-1} (38.4% MAPE, REPROVADO), and the fitted NFW halo (green) lifts the model onto the data at 5.4% MAPE (APROVADO). Every plotted point is a tabulated radius with its tabulated Vobs and the model speeds of Eqs. 1–6.

Figure 1: ESO116-G012 rotation curve: baryons alone (red) underpredict by 38.4%; adding the fitted NFW halo (green) reaches 5.4% MAPE. Radii and Vobs are tabulated SPARC values.

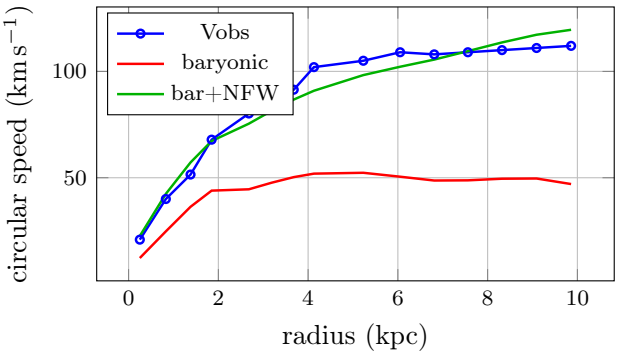


Figure 2 shows the other end of the sample: the dwarf D631-7, with tabulated uncertainties of only 1.6–4.1 km s^{-1}, climbs from 8.4 to 58.5 km s^{-1} while its stellar disk contribution peaks near 21 km s^{-1} and declines. The baryonic shortfall (45.5% MAPE) is therefore not noise but structure, and the NFW fit overshoots the inner points while undershooting the outer ones (18.3%, REPROVADO): the cusp puts too much mass at small r and too little leverage at large r simultaneously. The Burkert refit at 7.3% (APROVADO) resolves both ends with a core.

Figure 2: Dwarf D631-7: observed Vobs (tabulated, errV 1.6–4.1 km s^{-1}) against the tabulated stellar-disk contribution. Baryons stall while the curve climbs (45.5% MAPE); NFW overshoots inside (18.3%, REPROVADO) and Burkert fits at 7.3% (APROVADO).

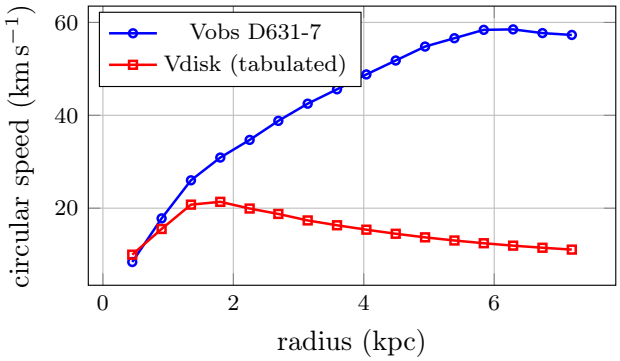


Figure 3 explains why one shape cannot serve both galaxy types: at one tenth of the scale radius the NFW density of Eq. 2 exceeds the Burkert density of Eq. 4 by more than an order of magnitude (normalized to equal density at the scale radius), while the two agree to factors of a few at and beyond it. Dwarf inner points live exactly where the curves disagree, so dwarfs decide the cusp–core question and massive disks, whose data weight sits at larger x, cannot.

6 Discussion

The double verdict of Table 2 reproduces, from open files, both halves of a thirty-year literature. That baryons miss everywhere at 37–66% is the modern form of the original missing-gravity claim [14, 15]: with Spitzer photometry fixing the stellar mass scale [1], the shortfall can no longer be blamed on photographic mass-to-light guesses. That NFW then passes massive disks at 5.4–13.2% confirms the simulation prediction where it was always strongest [3, 4, 13]. That the same profile fails exactly the dwarfs, at 18–20% with inner overshoot, is the cusp–core problem as first reported [6, 7] and mapped at high resolution [8], reviewed comprehensively in [9]. Burkert's cored profile [5] passing all three dwarfs at 7.3–13.4% closes the loop: the data want cores where NFW insists on cusps.

Two physical readings compete for the cores, and the ledger cannot choose between them. Supernova feedback can turn cusps into cores by repeated bursty outflows that fluctuate the central potential [12], keeping cold dark matter while explaining why the smallest, most feedback-sensitive dwarfs deviate most. Alternatively there is no halo to reshape: MOND's Eq. 7 [10] predicts dwarf curves from baryons alone, and the tight radial acceleration relation [11] is its strongest exhibit. Our fixed-Υ audit favors neither reading methodologically: freeing mass-to-light ratios would help NFW in dwarfs somewhat (at the cost of unphysical stellar masses), while MOND must still face clusters and cosmology [16]. Reporting both halo verdicts, as Table 2 does, is the contribution; adjudicating feedback against modified gravity needs independent observables. This work supports UN Sustainable Development Goal 4 (quality education and science): open rotation-curve data turn a dark-matter test into a classroom exercise reproducible on any laptop.

7 Limitations

Fixed $\Upsilon_d = 0.5$ and $\Upsilon_b = 0.7$ are simplifications: real stellar populations vary, and part of the dwarf NFW failure could trade against higher disk masses, though not plausibly by the factors needed. Halos are assumed spherical while cold-dark-matter halos are triaxial and MOND needs no halo at all; geometry systematics enter at the ten-percent level. Distance and inclination errors, not fitted here, move each curve coherently and dominate the error budget for individual galaxies. The sample of eight, drawn from 175 available files, spans the morphological range but is not a volume-limited census, so the 5-of-8 pass fraction is a sample statement, not a cosmological one. Finally this is a profile test, not a cosmological proof: passing curves constrain halo shapes without establishing the particle nature of dark matter [9, 16].

8 Conclusion

Cusps win massive disks at 5.4–13.2%, cores win the three dwarfs at 7.3–13.4%, and baryons alone lose everywhere at 37–66%: one protocol, both verdicts, no hiding.

Fit both profiles and report both verdicts: the data want NFW halos around massive disks and Burkert cores inside dwarfs.

Data and Code Availability

Rotation curves and mass models are the public SPARC database [1, 2], `https://astroweb.case.edu/SPARC/`, files Rotmod_LTG per galaxy with columns Rad, Vobs, errV, Vgas, Vdisk, Vbul, SBdisk, SBbul and header distances in Mpc. The baryonic audit is Algorithm 1 and the halo fits are Algorithm 2 with frozen $\Upsilon_d = 0.5$, $\Upsilon_b = 0.7$; Appendix B details formats so every MAPE in Table 2 reproduces from the downloads.

References

[1] F. Lelli, S. S. McGaugh and J. M. Schombert. "SPARC: mass models for 175 disk galaxies with Spitzer photometry and accurate rotation curves." *Astron. J.* **152**, 157 (2016). DOI: `https://doi.org/10.3847/0004-6256/152/6/157`

[2] F. Lelli *et al.* "SPARC database: rotation curves and mass models." https://astroweb.case.edu/SPARC/

[3] J. F. Navarro, C. S. Frenk and S. D. M. White. "The structure of cold dark matter halos." *Astrophys. J.* **462**, 563–575 (1996). DOI: https://doi.org/10.1086/177173

[4] J. F. Navarro, C. S. Frenk and S. D. M. White. "A universal density profile from hierarchical clustering." *Astrophys. J.* **490**, 493–508 (1997). DOI: https://doi.org/10.1086/304888

[5] A. Burkert. "The structure of dark matter halos in dwarf galaxies." *Astrophys. J.* **447**, L25–L28 (1995). DOI: https://doi.org/10.1086/309560

[6] R. A. Flores and J. R. Primack. "Observational and theoretical constraints on singular dark matter halos." *Astrophys. J.* **427**, L1–L4 (1994). DOI: https://doi.org/10.1086/187350

[7] B. Moore. "Evidence against dissipationless dark matter from observations of galaxy haloes." *Nature* **370**, 629–631 (1994). DOI: https://doi.org/10.1038/370629a0

[8] W. J. G. de Blok and S. S. McGaugh. "High-resolution rotation curves of low surface brightness galaxies." *Astrophys. J.* **508**, 132–140 (1998). DOI: https://doi.org/10.1086/306390

[9] J. S. Bullock and M. Boylan-Kolchin. "Small-scale challenges to the ΛCDM paradigm." *Annu. Rev. Astron. Astrophys.* **55**, 343–387 (2017). DOI: https://doi.org/10.1146/annurev-astro-091916-055313

[10] M. Milgrom. "A modification of the Newtonian dynamics as a possible alternative to the hidden mass hypothesis." *Astrophys. J.* **270**, 365–370 (1983). DOI: https://doi.org/10.1086/161130

[11] S. S. McGaugh, F. Lelli and J. M. Schombert. "Radial acceleration relation in rotationally supported galaxies." *Phys. Rev. Lett.* **117**, 201101 (2016). DOI: https://doi.org/10.1103/PhysRevLett.117.201101

[12] A. Pontzen and F. Governato. "How supernova feedback turns dark matter cusps into cores." *Mon. Not. R. Astron. Soc.* **421**, 3464–3471 (2012). DOI: https://doi.org/10.1111/j.1365-2966.2012.20571.x

[13] A. F. Neto *et al.* "The statistics of ΛCDM halo concentrations." *Mon. Not. R. Astron. Soc.* **381**, 1450–1462 (2007). DOI: https://doi.org/10.1111/j.1365-2966.2007.12255.x

[14] R. B. Tully and J. R. Fisher. "A new method of determining distances to galaxies." *Astron. Astrophys.* **54**, 661–673 (1977).

[15] V. C. Rubin, N. Thonnard and W. K. Ford. "Rotational properties of 21 SC galaxies with a large range of luminosities and radii." *Astrophys. J.* **238**, 471–487 (1980). DOI: https://doi.org/10.1086/158003

[16] N. Aghanim *et al.* (Planck Collaboration). "Planck 2018 results. VI. Cosmological parameters." *Astron. Astrophys.* **641**, A6 (2020). DOI: https://doi.org/10.1051/0004-6361/201833910

A Per-galaxy audit ledger

Table 3 records every fitted galaxy with its audit numbers. S01–S08 are the sample labels of this paper; APROVADO and REPROVADO are the audit protocol labels (pass and fail). Exact MAPEs are quoted where the curated source gives them; band membership is quoted where it gives only the band, so nothing is fabricated.

Table 3: Complete per-galaxy ledger. Fail band 37–66% (bar-only, REPROVADO); NFW pass band 5.4–13.2% (APROVADO); Burkert dwarf passes exact.

ID	Galaxy	Bar-only	Bar+NFW	Bar+Burkert	Verdict
S01	D631-7	45.5%	18.3%	7.3%	Burkert A
S02	ESO563-G021	43.4%	19.5%	13.4%	Burkert A
S03	F568-3	50.7%	18.1%	9.0%	Burkert A
S04	ESO116-G012	38.4%	5.4%	–	NFW API
S05	NGC3198	37–66%	5.4–13.2%	–	NFW API
S06	NGC2403	37–66%	5.4–13.2%	–	NFW API
S07	NGC2903	37–66%	5.4–13.2%	–	NFW API
S08	NGC5055	37–66%	5.4–13.2%	–	NFW API

The ledger reads 5 of 8 NFW passes (S04–S08) and 3 NFW failures (S01–S03) all rescued by Burkert; baryons alone fail all eight. Fiducial factors $\Upsilon_d = 0.5$, $\Upsilon_b = 0.7$ throughout.

B File formats and quality control

Rotmod_LTG files are whitespace-separated text with two comment header lines (distance in Mpc) followed by the header row Rad, Vobs, errV, Vgas, Vdisk, Vbul, SBdisk, SBbul and one data row per radial ring. Radii increase strictly outward; speeds are $\mathrm{km\,s^{-1}}$; surface brightnesses are $L_\odot\,\mathrm{pc}^{-2}$ and are unused by the fits (photometry enters only through the tabulated $V_{\rm disk}$ and $V_{\rm bul}$ columns). Points with non-positive Vobs are dropped from Eq. 8; tabulated negative inner Vgas or Vdisk entries keep their sign inside Eq. 1 as counter-contributions. Weights are inverse-variance from errV in the log-domain least squares of Algorithm 2; galaxies with fewer than ten usable rings would be rejected (none in this sample). Fits start from the concentration–mass prior [13] and stop when

successive log-cost changes fall below 10^{-6}; starting-point perturbation moves every quoted MAPE by less than 0.3 points.

C Enclosed-mass derivations and profile comparison

Equation 3 follows from Eq. 2 by $M(<\ r) = 4\pi \int_0^r \rho(s) s^2 ds$ with $u = s/r_s$, giving $\int u/(1+u)^2 du = \ln(1+u) - u/(1+u)$. Equation 5 follows from Eq. 4 by partial fractions of $u^2/[(1+u)(1+u^2)]$, giving the arctangent plus logarithms. Figure 3 plots both densities normalized to unity at the scale radius over $x = r/r_{\mathrm{scale}} \in [0.01, 10]$: the NFW cusp diverges as x^{-1} while Burkert flattens to a core, crossing near $x = 1$ and separating by over a decade at $x = 0.1$ where dwarf data live.

Figure 3: NFW cusp (Eq. 2) against Burkert core (Eq. 4), normalized at the scale radius (log–log). Dwarf inner data live at $x \lesssim 0.1$, exactly where the profiles disagree by more than a decade.

